

Article

X-ray Spectroscopy Based on Micro-Calorimeters at Internal Targets of Storage Rings

Marc Oliver Herdrich ^{1,2,3,*} , Daniel Hengstler ⁴ , Andreas Fleischmann ⁴ , Christian Enss ⁴ ,
Alexandre Gumberidze ³ , Pierre-Michel Hillenbrand ^{3,5} , Paul Indelicato ⁶ , Stephan Fritzsche ^{1,3,7} 
and Thomas Stöhlker ^{1,2,3} 

¹ Helmholtz-Institute Jena, Fröbelstieg 3, 07743 Jena, Germany

² Institute for Optics and Quantum Electronics, Friedrich Schiller University, 07743 Jena, Germany

³ GSI Helmholtz Center for Heavy Ion Research, Planckstraße 1, 64291 Darmstadt, Germany

⁴ Kirchhoff-Institute for Physics, Ruprecht Karls University, 69120 Heidelberg, Germany

⁵ Institute of Experimental Physics I, Justus-Liebig-University, 35392 Gießen, Germany

⁶ Laboratoire Kastler Brossel, Sorbonne Université, CNRS, ENS-PSL Research University, Collège de France, 75005 Paris, France

⁷ Institute for Theoretical Physics, Friedrich Schiller University, 07743 Jena, Germany

* Correspondence: m.o.herdrich@hi-jena.gsi.de

Abstract: With metallic-magnetic calorimeters (MMCs), promising detectors for high-precision X-ray spectrometry in atomic and fundamental physics experiments are available. In this work, we present a pilot experiment based on a *maXs*-30 type MMC-spectrometer for recording X-rays emitted in collisions of lithium-like uranium ions with a molecular nitrogen gas jet in the internal target of the ESR storage ring of the GSI. Sample spectra have been measured, and a multitude of X-ray transitions have been unambiguously identified. As a first test and for comparison with data recorded at an EBIT, the 2s Lamb shift in lithium-like uranium was estimated.

Keywords: atomic physics; metallic-magnetic calorimeters; high-precision X-ray spectroscopy; 2s Lamb shift



Citation: Herdrich, M.O.; Hengstler, D.; Fleischmann, A.; Enss, C.; Gumberidze, A.; Hillenbrand, P.-M.; Indelicato, P.; Fritzsche, S.; Stöhlker, T. X-ray Spectroscopy Based on Micro-Calorimeters at Internal Targets of Storage Rings. *Atoms* **2023**, *11*, 13. <https://doi.org/10.3390/atoms11010013>

Academic Editor: Izumi Murakami

Received: 31 October 2022

Revised: 6 January 2023

Accepted: 11 January 2023

Published: 14 January 2023



Copyright: © 2023 by the authors. Licensee MDPI, Basel, Switzerland. This article is an open access article distributed under the terms and conditions of the Creative Commons Attribution (CC BY) license (<https://creativecommons.org/licenses/by/4.0/>).

1. Introduction

In this work, we present the results of an ion-atom-collision experiment that was conducted at the ESR ion storage ring of the GSI Helmholtz-Centre for Heavy Ion Research, (Darmstadt, Germany). The measurement utilized a cryogenic calorimeter detector [1–3] for high-precision X-ray spectroscopy. Because of their unique working principles, metallic-magnetic calorimeters (MMCs) such as the *maXs*-series detectors developed in cooperation with the group of C. Enss at the KIP in Heidelberg combine many advantages over conventional energy-dispersive X-ray photon detectors. Several substantial achievements such as a spectral resolving power of $E/\Delta E > 6000$ [4], comparable to crystal spectrometers, over a broad spectral acceptance range of several orders of magnitude, comparable to semiconductor detectors, are associated with this promising technology. Additionally, it could be shown that MMC-detectors possess an excellent linearity $\Delta E/E < 0.16\%$ [5] as well as timing capability $\tau_0 < 100$ ns [6], making them particularly well-suited for high-precision X-ray studies in atomic and fundamental physics experiments involving heavy, highly charged ions. In the past, similar experiments have been conducted by various groups, for example, at electron-beam ion-traps (EBITs) [7–10], exploiting the advantages of calorimeter-based detectors for high-precision measurements. However, achieving this outstanding performance requires a shift from a conventional analog to a fully digital data processing and analysis pipeline. Therefore, a software framework for processing MMC data has been developed and improved over the course of multiple experiments that have been conducted on the GSI/FAIR campus in the past years. In the following, we present a test experiment aiming at the measurement of the 2s Lamb shift in lithium-like uranium

using an MMC detector (see Section 2). After a short discussion of the detector performance in Section 3, a detailed analysis and discussion of the recorded X-ray spectra follows in Section 4. In Section 5, finally, we conclude on the feasibility of using MMC detectors for atomic physics X-ray spectroscopy measurements.

2. Experiment

The experiment was conducted at the internal gas jet target of the experimental storage ring (ESR). It involved collisions between lithium-like U^{89+} projectiles at a beam energy of 75.91 MeV/u (calculated from the cooler voltage of the electron cooler $U_e = 41.64$ kV) on a molecular gas jet of N_2 . A detailed description of the experiment can be found in [11,12]. The maXs-30 detector (see [3] for details) was deployed in front of the 90° port of the target chamber at a distance of ≈ 1.5 m to the interaction point (see Figure 1). With an active detection area of around 10 mm^2 , this yields a solid angle of detection of 4.4×10^{-6} sr. A $25\text{ }\mu\text{m}$ -thin beryllium window was installed at the observation port, followed by a 120 cm-long pipe filled with helium in order to reduce the air gap to the detector to about 7 cm. Together with the X-ray entry window of the cold finger that connects the calorimeter to the cryostat (see [3]), an overall transmission of X-rays from the ESR of $\approx 40\%$ at 4 keV is expected. In order to perform an absolute energy calibration, a ^{241}Am source was placed in front of the detector before the experiment. The peaks corresponding to the five most prominent lines of the ^{241}Am spectrum (Np-L α_1 , Np-L β_1 , Np-L γ_1 , Np $\gamma(2 \rightarrow 1)$, and Np $\gamma(2 \rightarrow 0)$) were individually fit to a Gaussian peak model to determine their central positions. Then, a second-order polynomial regression was performed, matching the measured peak energies to their expected values [13] to find the quadratic energy calibration. A comparison between the calibrated central energies and their respective literature values gave rise to an average deviation of ± 3 eV.

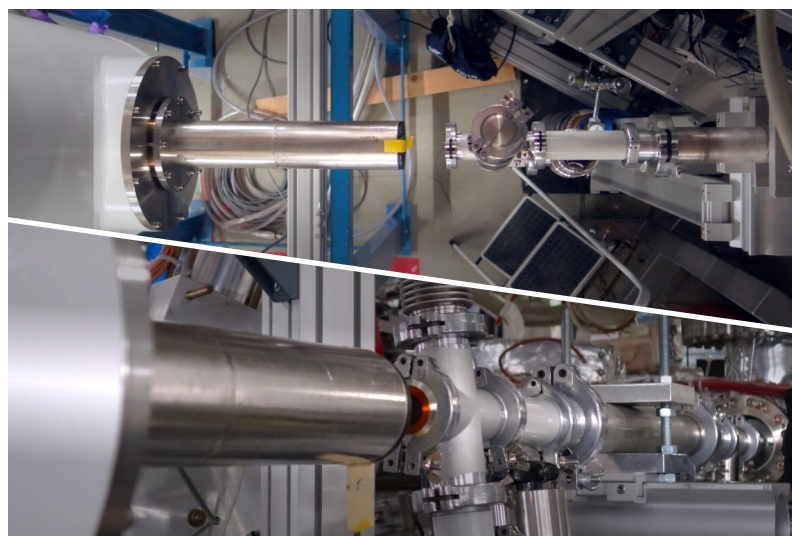


Figure 1. The two photos show the positioning of the MMC detector at the internal target of the ESR for the U^{89+} on N_2 collision experiment from different viewing angles. On the left, the cryostat, which is required to operate the calorimeters, is visible. On the right, the helium-filled tube can be seen, which bridges the air gap to the ESR gas jet target chamber, which is also visible in the bottom photo.

3. Detector Performance

Due to manufacturing-related magnetic impurities in the SQUID-based current sensors of the detector, the signals from multiple pixels were contaminated by a strong noise [3]. In order to mitigate this effect, only 11 of the 64 available channels with the highest resolution were taken into account for the analysis. At 59.5 keV photon energy, a resolution of 100 eV full-width half-maximum (FWHM) was observed by fitting the corresponding spectral feature to a Gaussian peak model. This broadening of the line compared to the

expected intrinsic energy resolution of the detector of ≈ 10 eV [3] can be attributed to drifts of the detector temperature that lead to corresponding variances in the amplification behavior. In the region of interest, the detector yielded a resolution of 36.7 eV FWHM (for energies < 26 keV). Besides the instrumental resolution, the measured lines are also impacted by Doppler broadening mostly stemming from the finite gas jet size. During the measurement period, the amplification of the detector jumped between three distinct regions. Therefore, each measured line consists of a main peak lined by two satellite peaks. In order to properly analyze the spectra of this experiment, a fit function consisting of three peaks with constant distance and relative height ratios to the main peak was constructed (see Equation (1)):

$$f(x) \equiv I_0 \cdot (G(x, E_0, \sigma) + i_1 \cdot G(x, e_1 E_0, s_1 \sigma) + i_2 \cdot G(x, e_2 E_0, s_2 \sigma)) \quad (1)$$

$$G(x, \mu, \sigma) \equiv \exp\left(-\frac{(x - \mu)^2}{2\sigma^2}\right) \quad (2)$$

Here, I_0 is the intensity of the main peak, and $i_{1,2}$ are the intensity ratios of the satellite peaks that depend on the time spent in each respective operation range. The central energy E_0 and the energy-dependent offsets $e_{1,2}$ (measured 0.98663 and 1.00681) agree with the results found by D. Hengstler (0.98682 and 1.00636) [3]. The observed instrumental resolution σ and peak width ratios $s_{1,2}$, however, differ from previous findings.

4. Experimental Data and Results

During the collision of U^{89+} ions with N_2 molecules, both the Coulomb excitation of the bound projectile electrons as well as the electron capture into excited states of the resulting U^{88+} ions were observed. The recorded spectra (see Figures 2–4) contain X-ray events from subsequent relaxations of electrons from excited states into as well as within the L-shell of lithium- (89+) and beryllium-like (88+) uranium ions (see Figure 5). In the following, the estimation of the 2s Lamb shift in lithium-like uranium is demonstrated, utilizing different combinations of measured transition energies.

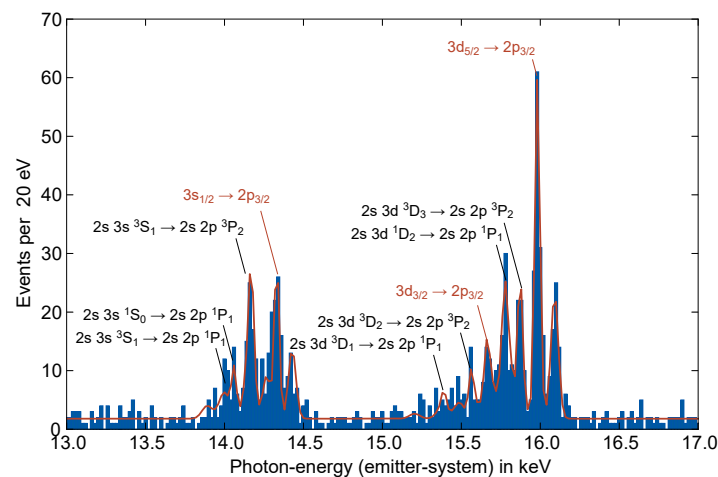


Figure 2. The spectrum contains X-ray transitions from the M- to the L-shell, resulting from the impact excitation of U^{89+} (red text) as well as the electron capture into excited states of U^{88+} (black text). For simplicity, the $1s^2$ term has been omitted from all given electronic configurations of U^{88+} ions. Overlaid is a fit to a model containing all identified lines (red line).

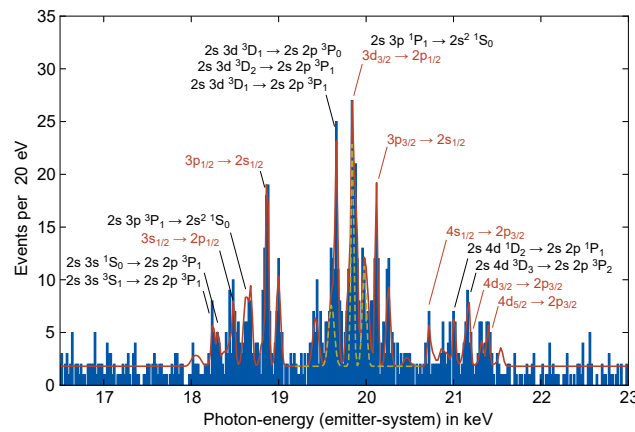


Figure 3. Shown is a spectrum that contains X-ray transitions of U^{89+} (red text) and U^{88+} (black text) from the N- and M-shells. Furthermore, a fit to a model consisting of all identified lines (red line) is presented. As an example, for the $3d_{3/2} \rightarrow 2p_{1/2}$ line, the individual fitting result is plotted (yellow, dashed line) in order to illustrate the discussed model function (Equation (1)) that takes into account the different operation points of the detector.

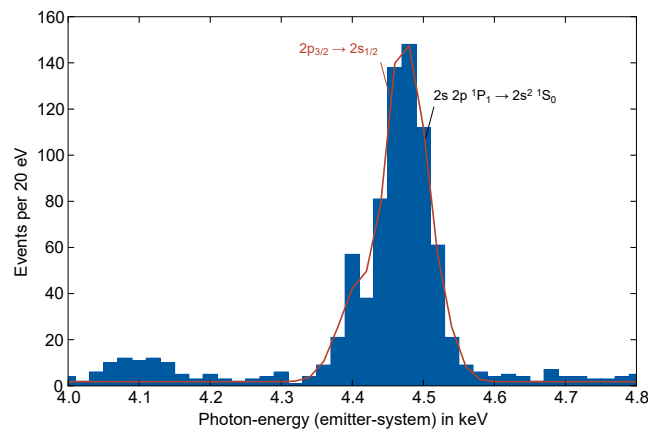


Figure 4. This spectrum contains X-ray transitions within the L-shell of U^{89+} (red text) as well as U^{88+} (black text). Additionally, a fit to a model containing all identified lines is plotted (red line).

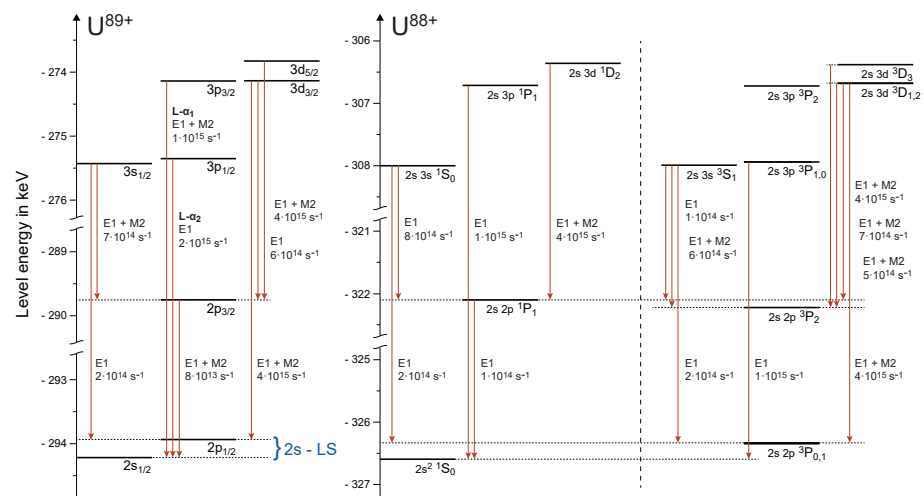


Figure 5. The two level schemes show the energy of the bound states of lithium-like (left) and beryllium-like uranium (right). Additionally, the X-ray transitions observed during the experiment are marked in the level schemes.

4.1. Transitions into the L-Shell

In order to identify the measured lines, the *Flexible Atomic Code* (FAC) [14] was used to predict the transition energies in U^{89+} and U^{88+} . Additionally, theoretical calculations for beryllium-like uranium and lithium-like uranium were performed including QED corrections [15]. Because of the comparably low beam energy, the non-radiative electron capture (NRC)-process is identified as being the dominant capture process. This matches the observation that no events stemming from the radiative electron capture (REC)-process are present in the spectra. For details about both processes and their cross-section properties related to the atomic number of the projectile Z_P and target Z_T as well as the kinetic energy of the projectile $E_{kin,P}$, we refer to the literature (see, for example, [16]). Since the excitation of a 1s electron into the M-shell, for example, is found to be ≈ 40 times less likely compared to the excitation of the 2s electron, only the latter case was considered in the analysis. Figures 2 and 3 present the measured spectra containing the X-ray transition from the M- and N- into the L-shell. Transitions from higher shells show too few statistics to be analyzed in a meaningful manner. After the identification of the lines, a fit with a model consisting of all identified lines described by the previously discussed model-function (Equation (1)) was performed. The positions of the most intense lines were then compared with their theoretical values in order to Doppler-correct the spectrum. The measured Doppler shift of 0.9235 ± 0.0004 presents a slight discrepancy to the expected value for the assumed experiment geometry (0.9251). However, due to the large uncertainties caused by the limited knowledge of the detector position relative to the interaction point, this is to be expected. Using multiple lines from the spectrum itself in order to determine the Doppler shift eliminates the need to rely on assumptions about the experiment geometry entirely. In the following, all transition energies refer to the Doppler-corrected spectrum. The given errors are an estimate for the statistical uncertainties using the assumption that $\Delta E_{stat} = \sigma / \sqrt{N}$, where N is the number of events of the respective spectral feature, and σ is the instrumental resolution. The overall systematic uncertainties stem from the calibration and the Doppler correction and amount to $\Delta E_{syst} / E \approx 8 \times 10^{-4}$.

In order to estimate the 2s Lamb shift of lithium-like uranium from the observed M- to L-shell transition energies, lines must be compared that target $2s_{1/2}$ and $2p_{1/2}$ as the final states of decay, respectively. Both $3p_{3/2} \rightarrow 2s_{1/2}$ and $3p_{1/2} \rightarrow 2s_{1/2}$ stem from relaxations into $2s_{1/2}$ and have good statistics. A direct determination of the difference in binding energy between $2s_{1/2}$ and $2p_{1/2}$ from the $3p_{3/2} \rightarrow 2s_{1/2}$ transition would require the observation of the $3p_{3/2} \rightarrow 2p_{1/2}$ transition. However, this decay channel is highly forbidden, with a decay rate two orders of magnitude lower than for the decay to $2s_{1/2}$; thus, it is not present in the recorded spectra. Instead, $3d_{3/2} \rightarrow 2p_{1/2}$ and $3s_{1/2} \rightarrow 2p_{1/2}$ are the only visible transitions into $2p_{1/2}$, although the latter is comparably weak. Using FAC to calculate the difference in binding energy between $E(3d_{3/2}) = 20,111.9$ eV and $E(3p_{3/2}) = 20,122.7$ eV together with their respective transitions to $2p_{1/2}$ and $2s_{1/2}$ (see Table 1) yields the 2s Lamb shift for U^{89+} :

$$\begin{aligned} E(2p_{1/2}) - E(2s_{1/2}) &= E(3p_{3/2} \rightarrow 2s_{1/2}) - E(3p_{3/2}) - E(3d_{3/2} \rightarrow 2p_{1/2}) + E(3d_{3/2}) \\ &= (284.3 \pm 5.1) \text{ eV} \end{aligned}$$

It should be mentioned that the estimation of the binding energies using FAC also contains large uncertainties up to the same order of magnitude as the measured uncertainties. In order to validate this method, the same calculation was performed for the $3p_{1/2} \rightarrow 2s_{1/2}$ line using $E(3p_{1/2}) = 18,861.5$ eV. The resulting value of (285.8 ± 4.9) eV matches the findings for $3p_{3/2} \rightarrow 2s_{1/2}$. A comparison with theoretical predictions (280.76 ± 0.14) eV [17] as well as with previous experimental findings [18–20] shows a reasonably good agreement for both results.

Table 1. This table lists the measured and Doppler-corrected L-shell-transitions used for the estimation of the 2s Lamb shift of uranium. The given errors represent the approximated statistical uncertainty of the lines (see the text for details). An additional systematic uncertainty of $\Delta E_{\text{sys}}/E \approx 8 \times 10^{-4}$ has to be taken into account. For comparison, the corresponding energy value calculated by FAC is given as well.

Transition U ⁸⁹⁺	ΔE_{exp} [eV] Emitter-System	ΔE_{theo} [eV] Calculation FAC
3d _{3/2} → 2p _{3/2}	15,660.6 ± 6.4	15,657.7
3d _{3/2} → 2p _{1/2}	19,844.1 ± 3.4	19,841.7
3p _{3/2} → 2s _{1/2}	20,117.6 ± 3.8	20,113.1
3p _{1/2} → 2s _{1/2}	18,868.7 ± 3.5	18,862.7

4.2. Transitions within the L-Shell

Besides transitions from higher shells into the L-shell, another peak structure at lower energies is observed that can be identified as intra L-shell transitions. The mixture of transitions from 2p_{3/2} → 2s_{1/2} of lithium-like uranium and 2s2p ¹P_{1/2} → 2s² ¹S₀ from the beryllium-like system is depicted in Figure 4. By applying the same multi-peak fit procedure as described in the previous sections, we find the transition energy of the 2p_{3/2} → 2s_{1/2} line to be (4459.85 ± 1.60 ± 3.57) eV (the first uncertainty term refers to the statistical uncertainty, and the second one refers to the systematic uncertainty). This is in excellent agreement with previous measurements (4459.37 ± 0.21) eV [21,22]. Utilizing the intra-shell transition presents an opportunity to calculate the 2s Lamb shift in lithium-like uranium without requiring additional knowledge about the 3d- and 3p-orbital-binding energies. The energy separation between 2p_{3/2} and 2p_{1/2} follows from the M- to L-shell transition $\Delta E(3d_{3/2} \rightarrow 2p_{3/2}) - \Delta E(3d_{3/2} \rightarrow 2p_{1/2})$. Combined with the $\Delta n = 0$ transition, the energy separation between the states 2p_{1/2} and 2s_{1/2} can be calculated (see Table 1):

$$\begin{aligned}
 E(2p_{1/2}) - E(2s_{1/2}) &= \Delta E(2p_{3/2} \rightarrow 2s_{1/2}) - (\Delta E(3d_{3/2} \rightarrow 2p_{1/2}) - \Delta E(3d_{3/2} \rightarrow 2p_{3/2})) \\
 &= (276.4 \pm 7.4) \text{ eV}
 \end{aligned}$$

Despite slightly lower statistics, this result also matches the findings described in the previous section and agrees well with both theory and previous experiments.

5. Conclusions and Outlook

In summary, the experiment presented in this work highlights the advantages of using an MMC detector for high-precision X-ray spectroscopy experiments. Multiple well-resolved lines in a broad spectral range can be recorded and calibrated within the same spectrum, exploiting the excellent linearity of the detector. This allows for a Doppler correction using the spectra themselves, thereby eliminating systematic errors resulting from uncertainties in the experiment setup. Furthermore, as demonstrated, opportunities arise to use different approaches to calculate the physical quantities of interest. The fairly large uncertainties stemming from temperature drifts and the overlapping amplification behaviors were dramatically reduced in later experiments by continuous calibration and temperature monitoring on a per-event basis. This was demonstrated, for example, in a recently performed experiment involving the deployment of maXs detectors at the electron cooler of the CRYRING@ESR storage ring [23]. Overall, cryogenic calorimeters such as the maXs-series detectors have proven to be an excellent tool for precision X-ray spectroscopy in the hard X-ray range, and more experiments using them as spectrometers at the storage rings of the new *Facility for Antiproton and Ion Research* (FAIR) are already planned.

Author Contributions: Analysis software, data analysis and presentation of the results: M.O.H.; Design, manufacturing and operation of microcalorimeter detectors: D.H., A.F. and all other participating members of the group of C.E.; Experiment at ESR: P.-M.H., T.G., A.G. and all participating members of GSI; Theory: P.I. and S.F.; Supervision, project administration and idea: T.S. All authors have read and agreed to the published version of the manuscript.

Funding: This work was financially supported by the European Union and the federal state of Thuringia via Thüringer Aufbaubank within the ESF project (2018 FGR 0080).

Data Availability Statement: No further research-data is available publicly at the moment.

Acknowledgments: This work was created within the SPARC collaboration.

Conflicts of Interest: The authors declare no conflict of interest. The funders had no role in the design of the study; in the collection, analyses, or interpretation of data; in the writing of the manuscript; or in the decision to publish the results.

References

1. Fleischmann, A. Magnetische Mikrokalorimeter: Hochauflösende Röntgenspektroskopie Mit Energiedispersiven Detektoren. Ph.D. Thesis, Ruprecht-Karls-Universität Heidelberg, Heidelberg, Germany, 2003.
2. Pies, C. maXs-200: Entwicklung Und Charakterisierung Eines Röntgendetektors Basierend Auf Magnetischen Kalorimetern Für Die Hochauflösende Spektroskopie Hochgeladener Ionen. Ph.D. Thesis, Ruprecht-Karls-Universität Heidelberg, Heidelberg, Germany, 2012.
3. Hengstler, D. Development and Characterization of Two-Dimensional Metallic Magnetic Calorimeter Arrays for the High-Resolution X-ray Spectroscopy. Ph.D. Thesis, Ruprecht-Karls-Universität Heidelberg, Heidelberg, Germany, 2017.
4. Geist, J. Bestimmung Der Isomereenergie von ^{229}Th Mit Dem Hochauflösenden Mikrokalorimeter-Array maXs30. Ph.D. Thesis, Ruprecht-Karls-Universität Heidelberg, Heidelberg, Germany, 2020.
5. Pies, C.; Schäfer, S.; Heuser, S.; Kempf, S.; Pabinger, A.; Porst, J.P.; Ranitsch, P.; Foerster, N.; Hengstler, D.; Kampkötter, A.; et al. maXs: Microcalorimeter Arrays for High-Resolution X-Ray Spectroscopy at GSI/FAIR. *J. Low Temp. Phys.* **2012**, *167*, 269–279. [[CrossRef](#)]
6. Fleischmann, A.; Enss, C.; Seidel, G.M. Metallic Magnetic Calorimeters. In *Cryogenic Particle Detection*; Enss, C., Ed.; Topics in Applied Physics, Springer: Berlin/Heidelberg, Germany, 2005; pp. 151–216. [[CrossRef](#)]
7. Thorn, D.B.; Gu, M.F.; Brown, G.V.; Beiersdorfer, P.; Porter, F.S.; Kilbourne, C.A.; Kelley, R.L. Precision Measurement of the K-Shell Spectrum from Highly Charged Xenon with an Array of X-Ray Calorimeters. *Phys. Rev. Lett.* **2009**, *103*, 0163001. [[CrossRef](#)] [[PubMed](#)]
8. Porter, F.S.; Adams, J.S.; Beiersdorfer, P.; Brown, G.V.; Clementson, J.; Frankel, M.; Kahn, S.M.; Kelley, R.L.; Kilbourne, C.A. High-resolution x-ray spectroscopy with the EBIT Calorimeter Spectrometer. *AIP Conf. Proc.* **2009**, *1185*, 454–457. [[CrossRef](#)]
9. Shen, Y.; Silver, E.; Hutton, R.; Zou, Y. The status of the micro-calorimeter at the Shanghai EBIT. *Phys. Scr.* **2011**, *2011*, 014060. [[CrossRef](#)]
10. Szypryt, P.; O’Neil, G.C.; Takacs, E.; Tan, J.N.; Buechele, S.W.; Naing, A.S.; Bennett, D.A.; Doriese, W.B.; Durkin, M.; Fowler, J.W.; et al. A transition-edge sensor-based X-ray spectrometer for the study of highly charged ions at the National Institute of Standards and Technology electron beam ion trap. *Rev. Sci. Instrum.* **2019**, *90*, 123107. [[CrossRef](#)] [[PubMed](#)]
11. Hillenbrand, P.M.; Hagmann, S.; Groshev, M.E.; Banaś, D.; Benis, E.P.; Brandau, C.; De Filippo, E.; Forstner, O.; Glorius, J.; Grisenti, R.E.; et al. Radiative Electron Capture to the Continuum in $\text{U}89^{+} + \text{N}_2$ Collisions: Experiment and Theory. *Phys. Rev. A* **2020**, *101*, 022708. [[CrossRef](#)]
12. Hillenbrand, P.M.; Lyashchenko, K.N.; Hagmann, S.; Andreev, O.Y.; Banaś, D.; Benis, E.P.; Bondarev, A.I.; Brandau, C.; De Filippo, E.; Forstner, O.; et al. Electron-Loss-to-Continuum Cusp in Collisions of $\text{U}89^{+}$ with N_2 and Xe. *Phys. Rev. A* **2021**, *104*, 012809. [[CrossRef](#)]
13. Chu, S.Y.F.; Ekström, L.P.; Firestone, R.B. Table of Radioactive Isotopes. 1999. Available online: <http://nucleardata.nuclear.lu.se/toi/> (accessed on 10 March 2021).
14. Gu, M.F. The Flexible Atomic Code. *Can. J. Phys.* **2008**, *86*, 675–689. [[CrossRef](#)]
15. Fritzsche, S. A fresh computational approach to atomic structures, processes and cascades. *Comput. Phys. Commun.* **2019**, *240*, 1–14. [[CrossRef](#)]
16. Eichler, J.; Stöhlker, T. Radiative Electron Capture in Relativistic Ion–Atom Collisions and the Photoelectric Effect in Hydrogen-like High-Z Systems. *Phys. Rep.* **2007**, *439*, 1–99. [[CrossRef](#)]
17. Yerokhin, V.A.; Indelicato, P.; Shabaev, V.M. Nonperturbative Calculation of the Two-Loop Lamb Shift in Li-Like Ions. *Phys. Rev. Lett.* **2006**, *97*, 0253004. [[CrossRef](#)] [[PubMed](#)]
18. Schweppe, J.; Belkacem, A.; Blumenfeld, L.; Claytor, N.; Feinberg, B.; Gould, H.; Kostroun, V.E.; Levy, L.; Misawa, S.; Mowat, J.R.; et al. Measurement of the Lamb Shift in Lithiumlike Uranium ($\text{U}89^{+}$). *Phys. Rev. Lett.* **1991**, *66*, 1434–1437. [[CrossRef](#)] [[PubMed](#)]

19. Brandau, C.; Kozhuharov, C.; Müller, A.; Shi, W.; Schippers, S.; Bartsch, T.; Böhm, S.; Böhme, C.; Hoffknecht, A.; Knopp, H.; et al. Precise Determination of the $2s_{1/2} - 2p_{1/2}$ Splitting in Very Heavy Lithiumlike Ions Utilizing Dielectronic Recombination. *Phys. Rev. Lett.* **2003**, *91*, 073202. [[CrossRef](#)] [[PubMed](#)]
20. Beiersdorfer, P.; Chen, H.; Thorn, D.B.; Träbert, E. Measurement of the Two-Loop Lamb Shift in Lithiumlike U 89+. *Phys. Rev. Lett.* **2005**, *95*, 0233003. [[CrossRef](#)] [[PubMed](#)]
21. Beiersdorfer, P.; Knapp, D.; Marrs, R.E.; Elliott, S.R.; Chen, M.H. Structure and Lamb Shift of $2s_{1/2} - 2p_{3/2}$ Levels in Lithiumlike U 89+ through Neonlike U 82+. *Phys. Rev. Lett.* **1993**, *71*, 3939–3942. [[CrossRef](#)] [[PubMed](#)]
22. Beiersdorfer, P. Spectral Measurements of Few-Electron Uranium Ions Produced and Trapped in a High-Energy Electron Beam Ion Trap. *Nucl. Instruments Methods Phys. Res. Sect. Beam Interact. Mater. Atoms* **1995**, *99*, 114–116. [[CrossRef](#)]
23. Pfäfflein, P.; Allgeier, S.; Bernitt, S.; Fleischmann, A.; Friedrich, M.; Hahn, C.; Hengstler, D.; Herdrich, M.O.; Kalinin, A.; Kröger, F.M.; et al. Integration of maXs-type Microcalorimeter Detectors for High-Resolution x-Ray Spectroscopy into the Experimental Environment at the CRYRING@ESR Electron Cooler. *Physica Scripta* **2022**, *97*, 0114005. [[CrossRef](#)]

Disclaimer/Publisher’s Note: The statements, opinions and data contained in all publications are solely those of the individual author(s) and contributor(s) and not of MDPI and/or the editor(s). MDPI and/or the editor(s) disclaim responsibility for any injury to people or property resulting from any ideas, methods, instructions or products referred to in the content.